Long-term models of oxidative stress and mitochondrial damage in insulin resistance progression

Erica J. Graham[a,1,*], Frederick R. Adler[a,b]

[a] *Department of Mathematics, College of Science, University of Utah, Salt Lake City, Utah, 84112*
[b] *Department of Biology, College of Science, University of Utah, Salt Lake City, Utah, 84112*

Abstract

Insulin resistance, characterized by a reduced cellular response to insulin, is a major factor in type 2 diabetes pathogenesis, with a complex etiology consisting of a combination of environmental and genetic factors. Oxidative stress, which develops through an accumulation of toxic reactive oxygen species generated by mitochondria, is believed to contribute to insulin resistance in certain tissues. We develop mathematical models of feedback between reactive oxygen species production and dysfunction in mitochondria to provide insight into the role of oxidative stress in insulin resistance. Our models indicate that oxidative stress generated by glucose overload accelerates irreversible mitochondrial dysfunction. These models provide a foundation for understanding the long-term progression of insulin resistance and type 2 diabetes.

Keywords: type 2 diabetes, superoxide

1. Introduction

Type 2 diabetes mellitus is central to a growing global epidemic of diabetes mellitus, constituting 90% of the estimated 471 million cases worldwide [1, 2]. The disease is characterized by excessively high plasma glucose concentrations,

*Corresponding author
Email addresses: ejgraha2@ncsu.edu (Erica J. Graham), adler@math.utah.edu (Frederick R. Adler)
[1] Present address: Department of Mathematics, College of Sciences, North Carolina State University, Raleigh, North Carolina, 27695

UU IR Author Manuscript

brought on by an imbalance between glucose and its major regulator, insulin. Insulin signals cells to uptake glucose from the blood. Reduced sensitivity to the insulin signal defines a state of insulin resistance (IR). IR increases the demand for insulin, to which pancreatic β cells, the cells that produce insulin, must respond by elevating insulin secretion. In type 2 diabetics, this β-cell compensation fails, and overt disease occurs [3].

The timeline of type 2 diabetes often spans decades [4, 5] and necessarily involves the development of β-cell dysfunction on a background of IR [6, 7]. Identifying the underlying mechanisms is difficult, with a combination of known environmental and genetic susceptibility factors [8, 9]. Common environmental influences include a high fat-high calorie diet, lack of physical activity, and obesity. Genetic predisposition can lead to defects in β-cell function, glucose sensing, insulin signaling, and appetite regulation. These factors, through stages not yet fully established [10, 11], promote a slow progression seemingly marked by irreversible damage. The goal of this paper is to model the mechanisms of irreversible damage contributing to IR, itself accepted to be the initial metabolic insult in type 2 diabetes.

The majority of insulin-stimulated glucose uptake occurs in skeletal muscle cells [12]. This uptake ultimately activates the mitochondrial electron transport chain (ETC) through which cellular energy as well as superoxide, a highly toxic reactive oxygen species (ROS), are created (Fig. 1). Superoxide is eliminated from mitochondria by the antioxidant manganese superoxide dismutase (MnSOD), which converts superoxide into the less toxic hydrogen peroxide. Mitochondrial superoxide, unlike hydrogen peroxide, cannot diffuse across mitochondrial membranes [13] and can accumulate in mitochondria. The resulting oxidative stress can damage resident proteins, including antioxidants, along with mitochondrial DNA (mtDNA), and can impair insulin signaling [14–16].

Superoxide can damage mtDNA via the oxidation of guanine bases, which creates molecular lesions that promote mtDNA mutation [20, 21]. Clonal mutations can also accumulate with age and dominate individual cells [22, 23]. Oxidative stress and substantial mtDNA mutation frequencies can result in

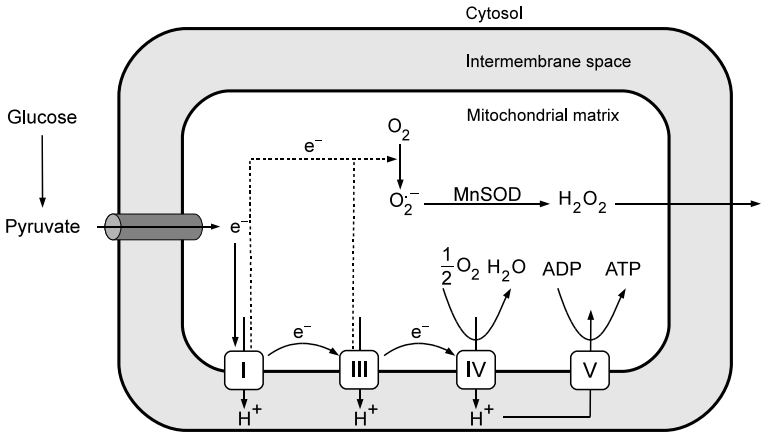

Figure 1. Oxidative phosphorylation and superoxide production. Intracellular glucose is broken down into pyruvate, which enters the mitochondrial matrix and produces pairs of electrons that flow through the electron transport chain (ETC). Each electron pair passes through ETC Complexes I and III in a series of oxidation/reduction reactions [17]. These reactions release energy that is used to pump protons from the matrix into the intermembrane space. This generates a potential energy gradient that is used to power ATP production. At Complex IV the electrons, along with free oxygen and protons in the mitochondrial matrix, are used to form water molecules [18]. When electrons leak from the ETC into the mitochondrial matrix, they can react with oxygen molecules to form superoxide [19]. Superoxide is detoxified by MnSOD, yielding hydrogen peroxide. ADP: adenosine diphosphate; ATP: adenosine triphosphate; e^-: electron; H^+: proton; H_2O: water molecule; H_2O_2: hydrogen peroxide; MnSOD: manganese superoxide dismutase; O_2: oxygen molecule; $O_2^{\cdot-}$: superoxide anion.

defective mitochondria, even under normal, and not necessarily pathological, circumstances [24]. Since 35% of genes encoded by mtDNA involve oxidative phosphorylation [25], ETC dysfunction can arise, in turn promoting superoxide overproduction [26] and further damage. Mitochondrial ROS can trigger targeted degradation, or mitophagy, of the organelle [27, 28], and damage may expose mitochondria to selective pressure [29], altering their replicative potential [30]. These processes can feed back to accelerate the process of damage whether within a single mitochondrion or in the population of mitochondria housed in a long-lived skeletal muscle cell.

Mitochondrial superoxide overproduction and damage, themselves influenced by genetic and environmental predisposition, lead to increased hydrogen peroxide in skeletal muscle cytosol. Although stress-activated signals responding to excessive cytosolic ROS certainly contribute to IR [31, 32], they may not initiate

IR. This work therefore highlights processes that are involved in long-term IR progression yet are not necessarily responsible for IR development.

In this paper we develop a series of mathematical models to describe oxidative stress and damage in skeletal muscle mitochondria. We focus on intracellular feedback mechanisms that contribute to progressive and irreversible damage associated with cellular IR. We present the model derivation, key results, and a discussion of implications for long-term modeling of IR and type 2 diabetes.

2. Methods

We develop a set of three models of three tightly coupled subsystems. The first tracks glucose and insulin in the plasma. The second follows the glucose within a cell and the resulting superoxide production and removal. The third tracks the consequences of mitochondrial selection within a cell.

Using the three subsystems we develop four models of how loss of mitochondrial function feeds back to the formation of ROS:

1. A mitochondrial inefficiency model (MIM) where a loss of function is linked directly to ROS.
2. A damaged mitochondria model (DMM) where ROS facilitate a process of intracellular mitochondrial selection that can lead to eventual takeover by damaged mitochondria prone to high ROS production.
3. A limited mitochondrial dysfunction model (LMDM) that includes both inefficiency and damage, where inefficiency is restricted to a class of damaged mitochondria.
4. A total mitochondrial dysfunction model (TMDM) that includes both inefficiency and damage, where inefficiency is not limited to damaged mitochondria.

2.1. The plasma glucose-insulin regulatory subsystem

To describe plasma dynamics of the glucose-insulin regulatory system (Fig. 2, Plasma), we modify the Topp et al. [33] βIG model for β-cell mass, $B(t)$, and

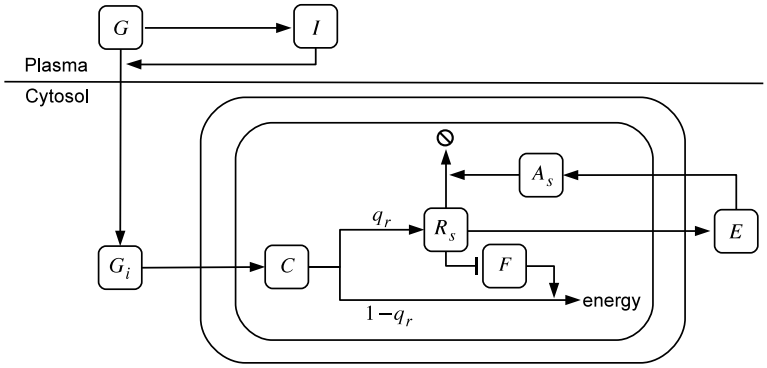

Figure 2. Diagram of the mitochondrial superoxide production model. Plasma insulin facilitates uptake of plasma glucose (G) into the cell (G_i). This leads to ETC activation (C) and ATP production. A fraction q_r of cellular respiration results in superoxide (R_s) formation, with the remainder dedicated to energy production. Superoxide inhibits mitochondrial function (F), thus impairing ATP production and increasing its own production. Superoxide also enhances MnSOD (A_s) production (E), which works to remove the anion from the mitochondrion.

concentrations of plasma glucose, $G(t)$, and insulin, $I(t)$, to include exogenous glucose input. We omit the effects of compensatory β-cell mass expansion by setting $B(t) = \beta$ for all t, giving

$$\frac{\mathrm{d}G}{\mathrm{d}t} = \sigma + h_g - (k_g + sI)G, \tag{1a}$$

$$\frac{\mathrm{d}I}{\mathrm{d}t} = h_i\beta\frac{G^2}{G^2 + G_h^2} - k_i I. \tag{1b}$$

Plasma glucose concentrations rise due to exogenous and endogenous sources. The parameter σ represents the external source of glucose, absorption from diet. The liver is the major contributor of internally-derived glucose, and its production rate is represented by h_g. Skeletal muscle cells remove glucose from the blood by insulin-independent and insulin-dependent means, corresponding to parameters k_g and s, respectively. The rate constant s is referred to as the insulin sensitivity parameter [33–35] and reflects the ability of target tissues such as skeletal muscle to respond to insulin at the post-receptor level. Insulin secretion is stimulated by glucose with a sigmoidal dose-response [36–39], with maximal rate h_i and half-saturation concentration G_h. Insulin is cleared at rate k_i.

2.2. The intracellular and mitochondrial subsystem

We summarize cellular respiration with a relatively small number of essential components (Fig. 2, Cytosol): intracellular glucose concentration (G_i), a representative ETC complex of proteins in the reduced state (C), mitochondrial superoxide (R_s), the antioxidant MnSOD (A_s), and an MnSOD translation signal (E). Glucose inputs lead, via the ETC, to the production of superoxide and the resulting generation of antioxidants and mitochondrial dysfunction. The subsystem is

$$\frac{\mathrm{d}G_i}{\mathrm{d}t} = v_1 \cdot sIG - k_{gi}G_i, \tag{2a}$$

$$\frac{\mathrm{d}C}{\mathrm{d}t} = v_2 k_{gi} G_i (C_{tot} - C) - k_c C[(1-q_r)F + q_r], \tag{2b}$$

$$\frac{\mathrm{d}R_s}{\mathrm{d}t} = k_c q_r C - k_{rs} R_s A_s - d_{rs} R_s^2, \tag{2c}$$

$$\frac{\mathrm{d}A_s}{\mathrm{d}t} = a_a E - q_a k_{rs} R_s A_s, \tag{2d}$$

$$\frac{\mathrm{d}E}{\mathrm{d}t} = a_e R_s (1-E) - k_e E. \tag{2e}$$

The entry of glucose into skeletal muscle cells via insulin-mediated glucose uptake from plasma (sIG) couples the plasma (1) and cellular (2) subsystems. The parameter v_1 is a conversion factor from plasma to cytosol, and we assume insulin-stimulated glucose uptake is distributed evenly among skeletal muscle cells. We also assume that glycolysis is first-order, with rate constant k_{gi}, to reduce the biological complexity of ATP production and utilization dynamics.

Complex proteins (C) in the oxidized state enter a reduced state immediately following glycolysis (Eq. (2b)). This one-to-one transfer yields a constant total pool, C_{tot}, of complex proteins that are either reduced (C) or oxidized ($C_{tot}-C$). Thus, glycolysis initiates the switch from oxidized to reduced state with rate $v_2 k_{gi} G_i (C_{tot} - C)$. The release of electrons is paired with ATP production, so that complex proteins return to an oxidized state with rate $k_c(1-q_r)F$, where q_r represents the small fraction [19] of cellular respiration that leads to the formation of superoxide. Oxidative respiration is retarded by the reduction of F, a slowly changing mitochondrial function variable whose form is specific to each of the models.

Electron leakage from the reduced ETC complex [25] is the primary source of superoxide (R_s) (Eq. (2c)). Efficient removal of superoxide requires a chemical reaction with MnSOD, A_s, at rate k_{rs}, but a much slower spontaneous dismutation can occur between two colliding superoxide anions at rate d_{rs}, where $d_{rs} \ll k_{rs}$ [40].

Nuclear translation of MnSOD requires an upregulation signal from a transcription factor, such as NF-κB, FoxO, and CREB proteins, which respond to elevated superoxide levels [41–43]. We therefore model both MnSOD and a representative translation signal in Eqs. (2d) and (2e). MnSOD is produced at maximal rate a_a, scaled by the strength of its translation signal, which ranges from zero to one. Although superoxide is eliminated by antioxidants, its highly toxic nature subjects mitochondria and their proteins, including a small fraction q_a of the antioxidant enzymes, to oxidative damage [44]. Translation signaling is activated by an increase in superoxide at rate a_e and decays exponentially to its inactive form, in the absence of superoxide.

We specify glucose input rate σ by introducing the reference parameter Δ_G, defined to be the difference between the average daily glucose concentration and the basal concentration G_0. Unlike σ, Δ_G is quantifiable from continuous glucose monitoring studies [45–47], which track frequent fluctuations in glucose over 24 hours. Redefining σ to be the rate of glucose input needed to maintain a constant glucose concentration of $G_0 + \Delta_G$, we derive σ from the glucose-insulin subsystem (1) and ignore the long-term feedback of the mitochondrial subsystem (2). Solving the system of algebraic equations

$$\begin{aligned} 0 &= \sigma + h_g - (k_g + sI)(G_0 + \Delta_G), \\ 0 &= h_i\beta \frac{(G_0 + \Delta_G)^2}{(G_0 + \Delta_G)^2 + G_h^2} - k_i I, \end{aligned} \tag{3}$$

for σ yields

$$\sigma = \frac{s\, h_i \beta (G_0 + \Delta_G)^3}{k_i[(G_0 + \Delta_G)^2 + G_h^2]} + k_g(G_0 + \Delta_G) - h_g. \tag{4}$$

To assess the influence of overnutrition on intracellular health independently of systemic metabolism, we assume that increased σ leads to higher rates of insulin-dependent, but not insulin-independent, uptake. We omit the possibility of metabolic changes prior to time $t = 0$ by imposing an initial state of equilibrium on the subsystem. As a result, glucose and insulin remain at their basal concentrations, G_0 and I_0, and glucose transfer from plasma into cells occurs with modified rate $\hat{s} = (\sigma + h_g - k_g G_0)/(G_0 I_0)$. The baseline sensitivity s used to compute σ implies that $\hat{s} = s$ only when $\sigma = 0$. It follows that $sIG = \hat{s} I_0 G_0 = \sigma + h_g - k_g G_0$. We modify Eq. (2a) in the mitochondrial subsystem to be

$$\frac{\mathrm{d}G_i}{\mathrm{d}t} = v_1(\sigma + h_g - k_g G_0) - k_{gi} G_i, \tag{5}$$

which contains an implicit representation of glucose-insulin adaptation, wherein the basal glucose concentration is maintained even when $\sigma > 0$. Δ_G is therefore independently responsible for changes in intracellular dynamics, and the updated model incorporates plasma subsystem (1) only as a constant input to Eq. (5).

2.3. Feedback in the mitochondrial subsystem

2.3.1. Mitochondrial inefficiency

Let $L(t)$ denote fractional mitochondrial inefficiency, assumed equal for all mitochondria. We model changes in L under the assumption that an altered balance, X, between superoxide and antioxidant capacity reduces mitochondrial efficiency. $L(t)$ therefore reflects the ROS-mediated damage to mitochondrial content that can lead to noticeable changes in mitochondrial respiratory activity.

$$\frac{\mathrm{d}L}{\mathrm{d}t} = \xi(1 - L)\frac{X^2}{X^2 + \lambda^2}, \quad \text{where } X = \frac{R_s/(R_s + A_s)}{R_{s0}/(R_{s0} + A_{s0})} - 1. \tag{6}$$

The basal ROS-antioxidant balance is defined to be $R_{s0}/(R_{s0} + A_{s0})$, where $R_{s0} = R_s(0)$ and $A_{s0} = A_s(0)$. The balance at time t is thus given by $R_s/(R_s + A_s)$, so that the ratio of the current to initial balance reflects overall changes to the antioxidant capacity of each mitochondrion. We subtract

1 in our definition of $X(t)$ so that a system in perfect balance does not contribute to mitochondrial inefficiency. A second-degree Hill function describes the sensitivity of mitochondrial inefficiency to superoxide; small increases in superoxide, coupled with moderate levels of MnSOD, minimally reduce mitochondrial efficiency due to damaged mitochondrial content such as lipids and proteins [28, 29, 48], whereas high superoxide concentrations and insufficient MnSOD reduce efficiency near the maximal rate ξ. We assume the loss of efficiency is limited by quality control mechanisms that target damaged mitochondrial content [49]. Hence, ξ is small relative to the other parameters in the mitochondrial subsystem. We thus define the mitochondrial inefficiency model (MIM) by representing mitochondrial function in Eq. (2b) as

$$F_{\mathrm{MIM}} = 1 - L. \tag{7}$$

2.3.2. Mitochondrial selection

The MIM assumes that all mitochondria in a given cell are functionally identical and respond uniformly to environmental changes. However, each cell harbors a population of hundreds of mitochondria that can differ in their degree of damage and genetics. In addition, intrinsic mitochondrial defects leading to ETC dysfunction do not necessarily translate into abnormal population dynamics [29]. We therefore explicitly consider a distinct stochastic process of heterogeneity that allows for differential population dynamics and function, to which we couple systems (1) and (2), in order to determine the effect of population-level feedback on superoxide production and damage.

Following the work of Kowald and Kirkwood [44], we address mitochondrial heterogeneity by defining two distinct mitochondrial subpopulations, undamaged and damaged, with respective sizes $M_0(t)$ and $M_1(t)$ at time t. At each mitochondrial division, we assume that only a transition from undamaged to damaged occurs, with probability μ (Fig. 3). A transition is defined to be the point at which a mitochondrion acquires class-specific characteristics arising from a myriad of underlying processes. These processes may include, but are

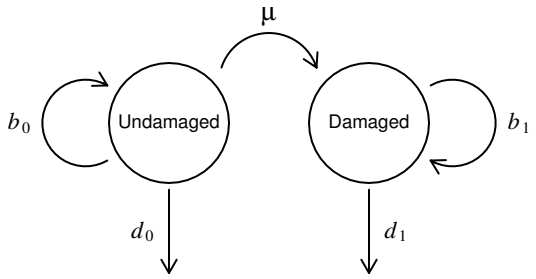

Figure 3. State transitions of the mitochondrial selection subsystem. Undamaged mitochondria transition to the damaged class with probability μ. Each class i replicates with rate b_i or turns over with rate d_i.

not limited to, effects of mutant mtDNA clonal expansion—which must accumulate to frequencies upwards of 60% before functional abnormalities are manifest [28, 50, 51]—mitochondrial swelling and membrane permeability [52, 53], and stress caused by an accumulation of damaged content in the mitochondrial matrix [28].

Assuming a constant total population size of $K = M_0(t) + M_1(t)$ allows us to describe total population dynamics entirely by a stochastic death process [54]. The fission and fusion events that determine mitochondrial population and functional dynamics *in vivo* are replaced by replicative birth events that depend probabilistically on the birth rates b_0 and b_1 and death rates d_0 and d_1 for undamaged and damaged mitochondria, respectively. The relationship between class-specific rates can vary. In a state of oxidative stress, mitochondrial ROS can signal mitophagy to reduce the number of damaged mitochondria [27, 53, 55], and damaged mitochondria may or may not have a replicative disadvantage relative to their undamaged counterparts [29, 30]. To account for multiple possibilities, we define

$$b_1 = (1 + s_r)b_0 \quad \text{and} \quad d_1 = (1 + s_m)d_0, \tag{8}$$

where the signs of s_r and s_m indicate the presence of an advantage (+) or disadvantage (−) in replication and turnover, respectively. When s_r and s_m are simultaneously zero, mitochondrial damage is neither directly beneficial nor

costly to the mitochondrion. We refer to this case as "null selection."

The average time between death events is $T = [d_0 M_0(t) + d_1 M_1(t)]^{-1}$. Setting $M_0(t) = K - M_1(t)$, let

$$p_j = \Pr\{M_1(t+\tau) = j-1 | M_1(t) = j\} \tag{9a}$$

$$q_j = \Pr\{M_1(t+\tau) = j+1 | M_1(t) = j\}, \tag{9b}$$

where $\tau \sim \text{Exp}(1/T)$. Respectively, p_j and q_j represent the net loss and gain of one damaged mitochondrion. It follows that $1 - p_j - q_j$ gives the probability of no change in a population of j damaged mitochondria due to the next death event. By definition,

$$p_j = \underbrace{\frac{d_1 j}{d_0(K-j) + d_1 j}}_{\text{damaged death}} \cdot \underbrace{\frac{(1-\mu) b_0 (K-j)}{b_0(K-j) + b_1 j}}_{\text{undamaged replacement}}, \tag{10a}$$

$$q_j = \underbrace{\frac{d_0(K-j)}{d_0(K-j) + d_1 j}}_{\text{undamaged death}} \cdot \underbrace{\frac{\mu b_0 (K-j) + b_1 j}{b_0(K-j) + b_1 j}}_{\text{damaged replacement}}. \tag{10b}$$

Let $\pi_j(t) = \Pr(M_1(t) = j)$ and define rates $\hat{p}_j = p_j/T$ and $\hat{q}_j = q_j/T$. Then the probability distribution of the number of mitochondria in the damaged class evolves according to the master equation [56]

$$\begin{aligned} \frac{\mathrm{d}\pi_0}{\mathrm{d}t} &= -\hat{q}_0 \pi_0 + \hat{p}_1 \pi_1, \\ \frac{\mathrm{d}\pi_j}{\mathrm{d}t} &= \hat{q}_{j-1}\pi_{j-1} - (\hat{q}_j + \hat{p}_j)\pi_j + \hat{p}_{j+1}\pi_{j+1}, \\ \frac{\mathrm{d}\pi_K}{\mathrm{d}t} &= \hat{q}_{K-1}\pi_{K-1} - \hat{p}_K \pi_K, \end{aligned} \tag{11}$$

for $1 \leqslant j \leqslant K-1$, and an initial distribution of $\pi_0(0) = 1$ and $\pi_j(0) = 0$ for $j \neq 0$.

With null selection, the mean time to fixation of the damaged type at the stationary distribution $\pi_K = 1, \pi_j = 0$ for $j \neq K$ is about 400 years given the parameters defined in Section 2.6 (see Appendix A). This slow timing, however,

neglects feedback from ROS. We include this feedback in the modified transition probability

$$\mu(t) = \mu_0 \left[1 + \rho \left(\frac{R_s(t)}{R_{s0}} - 1\right)\right]. \tag{12}$$

This function increases linearly with superoxide, from a value of μ_0 at the basal superoxide level R_{s0}. The slope ρ quantifies the effective strength of superoxide in signaling additional changes to mitochondrial integrity, under the assumption that damaged mitochondria house greater levels of ROS.

2.4. Models of mitochondrial dysfunction

As with the MIM, we develop subsequent models of mitochondrial dysfunction by specifying forms for the mitochondrial function variable F in Eq. (2b). To incorporate the influence of mitochondrial damage on ROS production, we assume that the damaged state can cause ETC dysfunction. Let $D(t)$ be the probability that any given mitochondrion is damaged, so that

$$D(t) = \frac{1}{K} \sum_{j=1}^{K} \pi_j(t) \cdot j. \tag{13}$$

We define the damaged mitochondria model (DMM) with

$$F_{\mathrm{DMM}} = 1 - D. \tag{14}$$

In the DMM, undamaged mitochondria are fully functional, whereas damaged ones are entirely dysfunctional.

Because all mitochondria are assumed to develop inefficiency uniformly, the remaining models probabilistically account for heterogeneities at the population level due to functional differences, with the mitochondrial function term F being the link between intramitochondrial processes and intracellular population dynamics. We define the limited mitochondrial dysfunction model (LMDM) with

$$F_{\mathrm{LMDM}} = (1 - D) + (1 - L)D = 1 - LD. \tag{15}$$

UU IR Author Manuscript

Model	Description	Mitochondrial function
MIM	mitochondrial inefficiency model	$F_{\mathrm{MIM}} = 1 - L$
DMM	damaged mitochondria model	$F_{\mathrm{DMM}} = 1 - D$
LMDM	limited mitochondrial dysfunction model	$F_{\mathrm{LMDM}} = 1 - LD$
TMDM	total mitochondrial dysfunction model	$F_{\mathrm{TMDM}} = (1 - L)(1 - D)$

Table 1. Overview of the four models. MIM: mitochondrial function determined by efficiency; DMM: mitochondrial function determined by undamaged mitochondria only; LMDM: mitochondrial function determined by undamaged or damaged, but efficient, mitochondria; TMDM: mitochondrial function determined by efficient, but undamaged, mitochondria.

In the LMDM, undamaged mitochondria are fully functional, whereas damaged ones are functional subject to residual efficiency. We define the total mitochondrial dysfunction model (TMDM) with

$$F_{\mathrm{TMDM}} = (1 - L)(1 - D). \tag{16}$$

In the TMDM, undamaged mitochondria are functional subject to residual efficiency, whereas damaged ones are entirely dysfunctional.

These models distinguish between two types of ROS-mediated abnormalities: (1) internal dysfunction, in which proteins and intramitochondrial damage affect electron transport, and (2) population-level dysfunction, in which the characterization of damage signals a change in mitochondrial population dynamics and additional defects in ETC activity. The models reflect a range of oxidative stress-mitochondrial damage feedback scenarios to be associated with the progression of IR. The LMDM allows the detrimental effect of damaged lipids, proteins and mutant mtDNA accumulation to only be carried out by damaged mitochondria, providing the most restrictive set of properties in feedback on superoxide production. On the other hand, the TMDM allows for substantial ETC dysfunction based on synergy between lost efficiency and mitochondrial damage. The MIM and DMM are simplified versions of these models, each representing a single cause of dysfunction. Table 1 summarizes the properties of the four models.

UU IR Author Manuscript

2.5. Initial conditions

We make the assumption that all variables begin at equilibrium with $\Delta_G = 0$ to derive the initial conditions and some of the parameters. Fasting plasma glucose and insulin concentrations in an individual with normal glucose metabolism are about 5.0 mM (90 mg/dl) and 60.0 pM, respectively [57]; therefore, we set $G_0 = 5.0$ mM and $I_0 = 60.0$ pM. Intracellular glucose concentrations are often difficult to determine [58], so we arbitrarily set $G_{i0} = 1.0$ mM. We assume that at steady-state, 20% of all complex proteins are in a reduced state. Based on a total concentration of 500 μM [59], we set $C_0 = 100\,\mu$M. Steady-state superoxide concentrations within the mitochondrial matrix are estimated to be between 10.0 and 200.0 pM [19, 60]. Taking the minimum of the interval, we set $R_{s0} = 10^{-5}\,\mu$M. The steady-state concentration of MnSOD has been measured to be about $A_{s0} = 5.0\,\mu$M [40]. 20% of MnSOD translation activity is assumed to be engaged initially, so that $E_0 = 0.2$. We assume mitochondria have not yet acquired dysfunction at $t = 0$; thus, we set $L_0 = 0$ and $\pi_0(0) = 1$, $\pi_j(0) = 0$ for $j \neq 0$.

2.6. Parameter estimates

In this section, we discuss the choices for all parameters in the model, based our initial steady-state assumption.

a_a, *MnSOD production.* We assume that the maximal level of MnSOD production achieves the steady-state antioxidant concentration after 2 hours. We therefore compute $a_a = A_{s0}/120 = 0.04167$ μM min^{-1}.

a_e, *MnSOD signal activation.* The steady-state concentration of superoxide, R_{s0}, is assumed to maximally stimulate MnSOD production activity within 6 hours. The rate of signal activation is thus $a_e = 1/(360R_{s0}) = 277.78$ min^{-1}.

b_0, *undamaged mitochondrial growth.* We assume growth of the undamaged mitochondrial class balances its turnover, so that $b_0 = 0.07$ d^{-1}.

b_1, *damaged mitochondrial growth.* With null selection, we assume damaged mitochondria replicate at the same rate as undamaged ones, so that $b_1 = 0.07$.

UU IR Author Manuscript

Parameter	Description	Value	Units	Reference
a_a	MnSOD production rate	0.04167	min^{-1}	
a_e	MnSOD signal activation rate	277.78	min^{-1}	
β	β-cell mass	1000	10^6 cells	[34]
b_0	undamaged mitochondrial growth rate	0.07	d^{-1}	$*$
b_1	damaged mitochondrial growth rate	0.07	d^{-1}	$*$
C_{tot}	total ETC complex protein concentration	500	μM	[59]
Δ_G	average daily change in glucose	0.0 – 3.0	mM	[46]
d_0	undamaged mitochondrial turnover rate	0.07	d^{-1}	[24, 55]
d_1	damaged mitochondrial turnover rate	0.07	d^{-1}	$*$
d_{rs}	spontaneous superoxide dismutation rate	12.0	μM^{-1} min^{-1}	[13]
G_h	half-maximal glucose stimulation	9.0	mM	[34, 61]
h_g	hepatic glucose production rate	0.12	mM min^{-1}	$*$
h_i	insulin production rate	0.03527	$(10^6 \text{ cells})^{-1}$ min^{-1}	$*$
K	total mitochondrial population size	500	mitochondria	[17, 62]*
k_c	cellular respiration rate	240.0	min^{-1}	$*$
k_e	MnSOD signal deactivation rate	0.01111	min^{-1}	$*$
k_g	insulin-independent uptake rate	0.018	min^{-1}	[12]*
k_{gi}	rate of glycolysis	0.007653	min^{-1}	$*$
k_i	insulin clearance	0.1386	min^{-1}	[63]
k_{rs}	superoxide dismutation rate	1.2×10^5	μM^{-1} min^{-1}	[13]
λ	half-maximal inefficiency stimulus	10	#	
$\mu\,(\mu_0)$	damage transition probability (baseline)	10^{-4}	#	
q_a	MnSOD damage probability	0.001389	#	$*$
q_r	fractional superoxide production	2.5×10^{-4}	#	
ρ	superoxide-to-damage feedback strength	0.25	#	
s	baseline insulin sensitivity	10^{-4}	pM^{-1} min^{-1}	[34]*
v_1	glucose distribution factor	0.25510	#	[64, 65]*
v_2	ETC conversion factor	7840	mM^{-1}	[64, 66]*
ξ	rate of lost mitochondrial efficiency	5×10^{-5}	d^{-1}	

Table 2. Parameter values for the models. Derived quantities denoted by $*$.

β, *β-cell mass.* β-cell mass is estimated to be on the order of 10^9 cells in [34]. In millions of cells, we set $\beta = 1000$.

C_{tot}, *total ETC protein concentration.* Ubiquinone has been used to represent a collective ETC complex in a model of superoxide production in rats [59]. Postmortem investigations have reported comparable concentrations of ubiquinone in rats and humans [67]. We assume a total ETC concentration of 500 μM [59].

d_0, *undamaged mitochondrial turnover.* The half-life of mitochondria is estimated to be between 10 and 25 days [68]. With a 10-day half-life, we take d_0 to be $d_0 = \ln 2/10 \approx 0.07$ d^{-1}.

d_1, *damaged mitochondrial turnover.* With null selection, we assume turnover of damaged mitochondria occurs at the same rate as undamaged mitochondria, so that $b_1 = 0.07$.

Δ_G, *average daily change in glucose.* Continuous glucose monitoring studies [46] give a maximum average daily change in glucose of 4 mM. This extreme case typically corresponds to individuals with a diagnosis of diabetes mellitus or other metabolic disorder. We restrict ourselves to a range of 0.0 mM to 3.0 mM.

d_{rs}, *spontaneous superoxide dismutation.* The collision of two superoxide anions results in spontaneous dismutation. This event is significantly less likely than contact between superoxide and MnSOD. The rate of spontaneous superoxide dismutation has been measured to be 12 μM^{-1} min^{-1} [13].

G_h, *half-maximal glucose stimulation.* Dose-response studies [37, 38, 61] suggest that glucose stimulates insulin secretion in a sigmoidal manner, with half-maximal stimulation occurring between 5 mM and 12 mM. Following [34], we therefore use $G_h = 9$ mM.

K, *total population size.* Mammalian cells have, on average, between 10^3 and 10^4 copies of mtDNA, with each mitochondrion housing 2 – 10 copies [17]. Assuming a skeletal muscle cell copy number of 5000 with a per-mitochondrion number of 10, as in [62], we set $K = 500$, in line with the 100 to 1000 mitochondria estimate of mammalian cells [20].

k_g, *insulin-independent uptake.* Under basal conditions, about 75% of glucose uptake occurs via insulin-independent means [12]. At $t = 0$ and with $\Delta_G = 0$, $\mathrm{d}G/\mathrm{d}t = h_g - k_g G_0 - sG_0 I_0$. We therefore assume $k_g = 3sI_0 = 0.018$ min^{-1}.

k_i, *insulin clearance.* The half-life of insulin, under the assumption of first-order clearance, is 5 minutes [63]. We therefore use $k_i = \ln 2/5 = 0.03527$ min^{-1}.

k_{rs}, *superoxide dismutation.* MnSOD interacts with superoxide at a rate $\sim \mathcal{O}(10^9)$ M^{-1} s^{-1} [13, 40]. As in [40], we use $k_{rs} = 1.2 \times 10^5$ $\mu\mathrm{M}^{-1}$ min^{-1}.

λ, *half-maximal inefficiency stimulus.* We assume mitochondrial inefficiency is exacerbated by a considerable imbalance between superoxide and MnSOD. We set $\lambda = 10$, which corresponds to an 11-fold increase in the relative superoxide:MnSOD balance.

$\mu\,(\mu_0)$, *damage transition probability.* We assume the baseline probability that damage-specific characteristics appear in mitochondria is small, with $\mu_0 = 10^{-4}$.

q_r, *fractional superoxide production.* The fraction of oxidative phosphorylation in isolated mitochondria resulting in superoxide production has been found to lie between 0.001 and 0.04 [69–71]. It is estimated that *in vivo* this percentage is much smaller [19, 72], and we thus set $q_r = 2.5 \times 10^{-4}$.

ρ, *strength of superoxide feedback on mitochondrial damage.* We have taken this parameter to range between 0 and 1, which limits the strength of feedback to the ratio of superoxide concentration to the steady-state level. In model results, we set $\rho = 0.25$.

s, *baseline insulin sensitivity.* In the case of constant insulin sensitivity, we use a value of 10^{-4} pM^{-1} min^{-1}, as in [34].

v_1, *glucose distribution factor.* The standard quantity of plasma is 5 L. It is estimated that there are roughly 300 skeletal muscles in the human body, each with $3-4\times10^5$ individual fibers [65]. Combined, we assume 10^8 skeletal muscle fibers consume plasma glucose. Myofibers may have a diameter in the range from 10 to 100 μM and a length in the 5 to 10 cm range [64]. Assuming a cylindrical

geometry with a 50-μM diameter and a height of 10 cm, we estimate a total fiber volume of 1.96×10^{-7} L/cell. We therefore calculate the glucose distribution factor between plasma and intracellular environment to be $5/19.6 = 0.2551$.

v_2, *ETC conversion factor.* It is estimated that up to 20% of skeletal muscle cell volume comprises mitochondria [64]. With a skeletal muscle cytosolic volume of 1.96×10^{-7} L (see derivation of v_1) and a mitochondrial population of 500, an individual mitochondrial matrix volume of 0.05 μm^3 or 5×10^{-11} L yields a total volume that is between 5% and 10% of the cellular volume, once the volume of the intermembrane space is taken into account. Using this information, we calculate $v_2 = 7840$ mM^{-1}.

ξ, *loss of mitochondrial efficiency.* We assume the net loss of mitochondrial efficiency due to damaged mitochondrial content occurs at the low maximal rate 5×10^{-5} d^{-1}.

By imposing an initial steady-state for $\Delta_G = 0$ in each model, we derive the remaining parameters: hepatic glucose production rate, $h_g = k_g G_0 + s G_0 I_0 = 0.12$; insulin production rate, $h_i = k_i I_0 (G_0^2 + G_h^2)/(\beta G_0^2) = 0.03527$; cellular respiration rate, $k_c = (k_{rs} R_{s0} A_{s0} + d_{rs} R_{s0}^2)/(q_r C_0) = 240.0$; MnSOD signal deactivation rate, $k_e = a_e R_{s0}(1 - E_0)/E_0 = 0.01111$; glycolytic rate, $k_{gi} = v_1 s G_0 I_0 / G_{i0} = 0.00765$; MnSOD damage probability, $q_a = a_a E_0/(k_{rs} R_{s0} A_{s0}) = 0.00139$. Table 2 summarizes the parameter values used in Section 3.

3. Results

We solve each model numerically over a 100-year period and compare results for values of Δ_G, the measure of excess glucose intake, between 0.0 mM and 3.0 mM. In Sections 3.1–3.3, results are reported for null selection where applicable. In Section 3.4, we consider alternate forms of mitochondrial selection.

3.1. Time-dependent effects of glucose excess

For each model, cellular glucose seems constant over time, but attains a high set point with high Δ_G. With sufficiently high Δ_G, the feedback initiates

an increase in mitochondrial inefficiency or damage, and in superoxide levels, always with a decrease in antioxidant levels despite increases in the translation activity. Fig. 4 shows results with the MIM, but the others are qualitatively similar (results not shown).

3.2. Slow feedback and oxidative stress

In Fig. 5, we use parametric plots of loss of mitochondrial function $(1 - F)$ against superoxide levels to display the feedback. The four models differ in the qualitative loss of mitochondrial function. The TMDM produces the highest level of overall mitochondrial dysfunction and oxidative stress and the most rapid progression for different Δ_G.

3.3. Structural uniformity across models

Fig. 6 illustrates the changes in superoxide over time relative to initial Δ_G-adjusted levels for the four models. A single curve determines the relationship between superoxide production and mitochondrial abnormalities. Δ_G correlates with more rapid progress along the curve, but the curve itself is uniform across all models (Fig. 6, starred curves). This suggests that individuals with different Δ_G behave similarly, but on different time scales.

3.4. Effects of mitochondrial selection

To determine the role of selection parameters s_m and s_r in the behavior of the DMM, LMDM, and TMDM, we obtain model solutions for several parameter combinations. Fig. 7(a) illustrates the s_m-s_r parameter space, subdivided into six qualitative regions ($R1$–$R6$). Each region is characterized by a combination of three properties: the sign of s_m; the sign of s_r; and, the sign of $s_r - s_m$.

We choose representative parameters within each subregion, and determine the superoxide concentration and mitochondrial dysfunction at year 45 through numerical solutions (Figs. 7(b)–(d)). Variation of the selection parameters does not alter the shape of the null-selection parametric curves. The LMDM is least sensitive, and the TMDM most sensitive, to changes in s_m and s_r. Oxidative

UU IR Author Manuscript

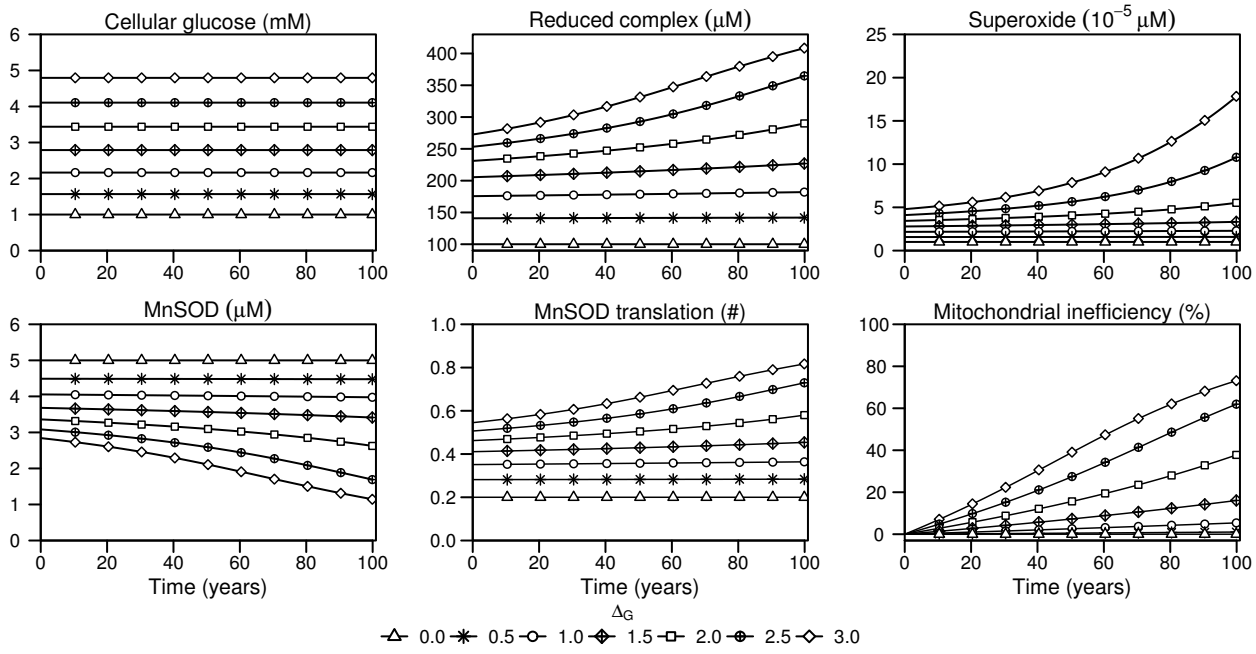

Figure 4. Time-dependent trajectories of the MIM intracellular variables. Plasma trajectories for glucose (G) and insulin (I) remain constant over time, as described in Section 2.1. With Δ_G-dependent insulin sensitivity, basal levels of each intracellular variable are adjusted accordingly. After the adjustment, intracellular glucose (G_i) remains constant over time, with higher concentrations obtained by increasing Δ_G. The concentration of complex proteins in a reduced state (C), superoxide (R_s), MnSOD translation activity (E), and mitochondrial inefficiency (L) are all elevated and rise more quickly with Δ_G. The concentration of MnSOD (A_s) reflects the reverse dynamics. Δ_G is negatively correlated with MnSOD level, which declines faster with increasing Δ_G. For $\Delta_G \leqslant 1$, adjusted baseline levels prevail over a lifetime.

UU IR Author Manuscript

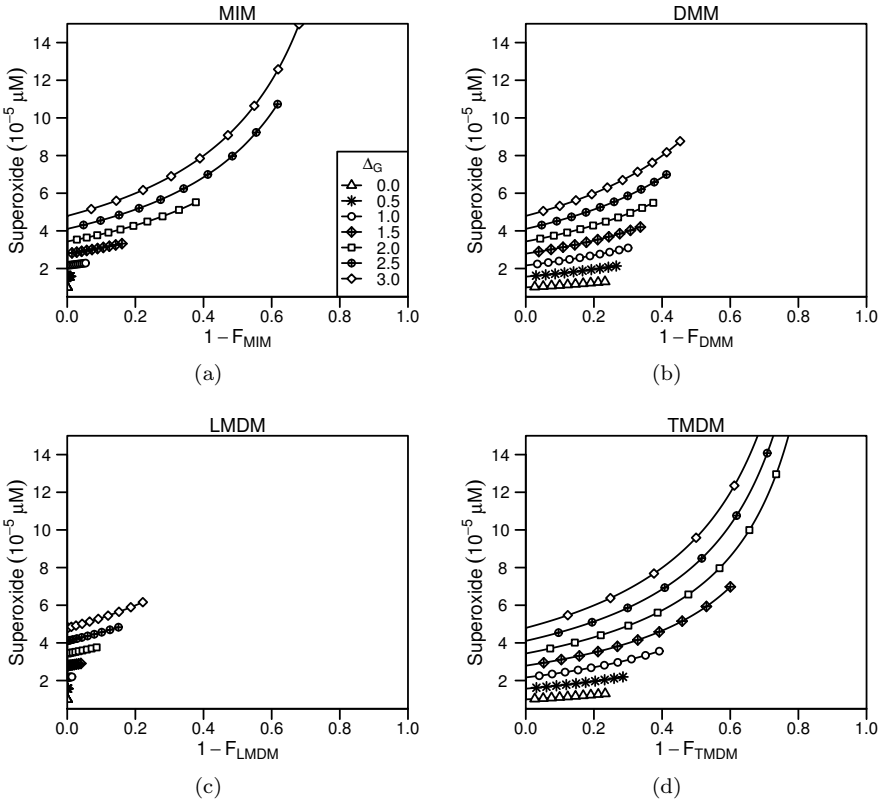

Figure 5. Relationship between superoxide and slow feedback in the models. Symbols indicate 10-year increments. Null selection implemented where applicable. (a) Mitochondrial inefficiency model. Mitochondrial inefficiency, $L = 1 - F_{\mathrm{MIM}}$, and oxidative stress increase more quickly with larger Δ_G. No change is observed for $\Delta_G = 0$. (b) Damaged mitochondria model. The fraction of damaged mitochondria, $D = 1 - F_{\mathrm{DMM}}$, and oxidative stress increase more quickly with Δ_G. Compared to the MIM, superoxide increases at slower rates when $\Delta_G \geqslant 2$, but more quickly when $\Delta_G < 2$. (c) Limited mitochondrial dysfunction model. Mitochondrial dysfunction, $1 - F_{\mathrm{LMDM}}$, and oxidative stress increase more quickly with larger Δ_G. Compared to the MIM and DMM, superoxide increases at slower rates for $\Delta_G > 0$. No change is observed for $\Delta_G = 0$. (d) Total mitochondrial dysfunction model. Mitochondrial dysfunction, $1 - F_{\mathrm{TMDM}}$, and oxidative stress increase more quickly with larger Δ_G. Although superoxide increases more quickly for all Δ_G compared to the other models, the rate is essentially identical to the DMM when $\Delta_G = 0$.

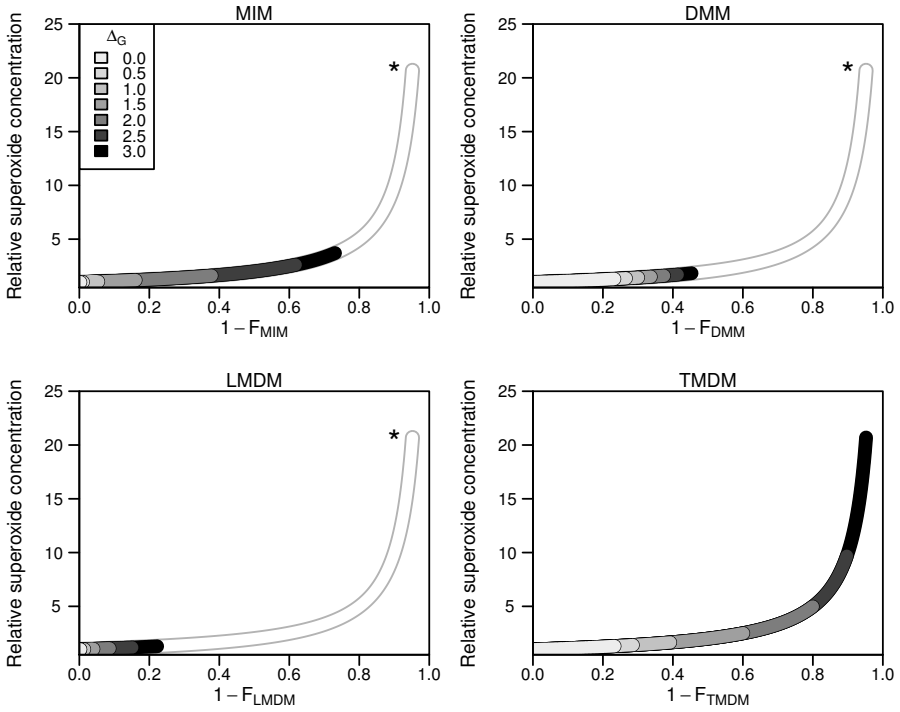

Figure 6. Model summary and comparison. Null selection implemented where applicable. Superoxide concentrations relative to Δ_G-adjusted levels are plotted against respective mitochondrial dysfunction variables for a range of Δ_G. Δ_G hastens the progression of oxidative stress along a predetermined curve. Parametric curves of the loss of mitochondrial function terms $1 - F$ against relative superoxide concentrations follow identical paths. *Indicates comparison curve reproduced from TMDM ($\Delta_G = 3.0$, darkest curve in *bottom right* panel).

stress and mitochondrial abnormalities increase more quickly for parameters in regions $R1$, $R2$, and $R3$ relative to the null-selection case, but more slowly for parameters in $R4$, $R5$, and $R6$.

We therefore reduce the number of qualitative regions of the s_m-s_r parameter space to two, $s_r > s_m$ and $s_r < s_m$, denoted Zone 1 and Zone 2, respectively. We use age maps to describe the age at which an arbitrarily chosen superoxide concentration of $10^{-4}\,\mu$M has been reached or exceeded for various Δ_G (2.0–3.0 mM), s_m, and s_r, with the difference in birth or death rates between mitochondrial classes limited to 10% (Fig. 8). The value of $s_r - s_m$ determines the age at which the threshold is exceeded, which is dramatically reduced when $s_r - s_m < 0$. This suggests that a replicative advantage can overcome targeted degradation of damaged mitochondria when the percent increase in growth is greater than that in turnover (Zone 1), resulting in accelerated superoxide production and mitochondrial dysfunction. On the other hand, the threshold is almost never exceeded if the reverse is true (Zone 2). For each Δ_G, the average age to reach threshold Zone 1 decreases. The threshold is never reached in the LMDM for $\Delta_G \leqslant 2.0$. The TMDM is the only model leading to excessive superoxide for parameters are contained in Zone 2.

4. Discussion

The mitochondrion, as a source of ROS, is thought to be an important factor in both aging [21, 44, 73, 74] and in skeletal muscle insulin resistance (IR) [14, 25]. Our models suggest that slow accumulation of damage in mitochondria contributes to age-related elevations in oxidative stress in skeletal muscle and is accelerated by a positive feedback loop. ROS promote mitochondrial inefficiency and damage, which lead to defective electron transport, increased ROS production, and further mitochondrial dysfunction. These models support a role for mitochondria in sustained IR.

A major output of each model is mitochondrial superoxide. Hydrogen peroxide, a derivative of superoxide, can freely diffuse into the cytosol and activate

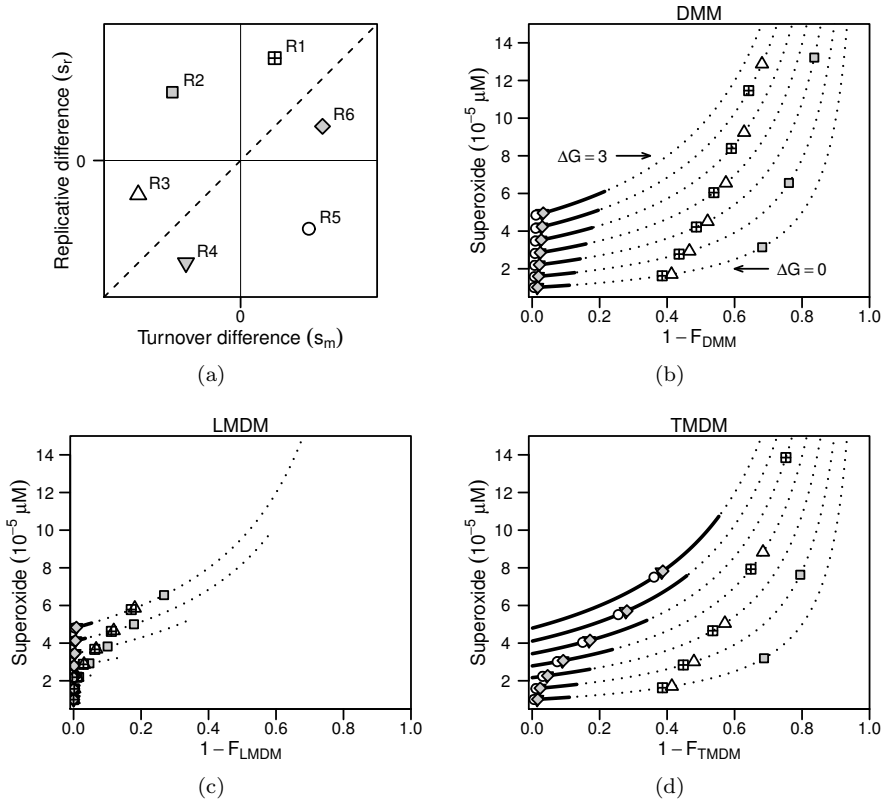

Figure 7. Response to mitochondrial selection. (a) s_m-s_r parameter space, indicating fractional difference between damaged and undamaged turnover and replication rates, respectively. Qualitative subregions denoted $R1$–$R6$. (b) DMM, (c) LMDM, and (d) TMDM responses to selection parameters for various Δ_G. Bottommost curves correspond to $\Delta_G = 0.0$, topmost to $\Delta_G = 3.0$. Symbols denote representative parameter combinations from the corresponding subregion at year 45. Bold lines (—): 45-year trajectory for null selection; dotted lines (· · ·): extended path produced by $R2$ parameters. Superoxide increases more quickly for parameters in $R1$, $R2$, and $R3$, with the most dramatic elevations produced by $R3$ parameters. Slower increases observed for parameters in $R4$, $R5$, and $R6$. Parameter combinations: $R1$. $s_m = 0.05$, $s_r = 0.06$; $R2$. $s_m = -0.01$, $s_r = 0.01$; $R3$. $s_m = -0.05$, $s_r = -0.04$; $R4$. $s_m = -0.05$, $s_r = -0.06$; $R5$. $s_m = 0.01$, $s_r = -0.01$; $R6$. $s_m = 0.05$, $s_r = 0.04$.

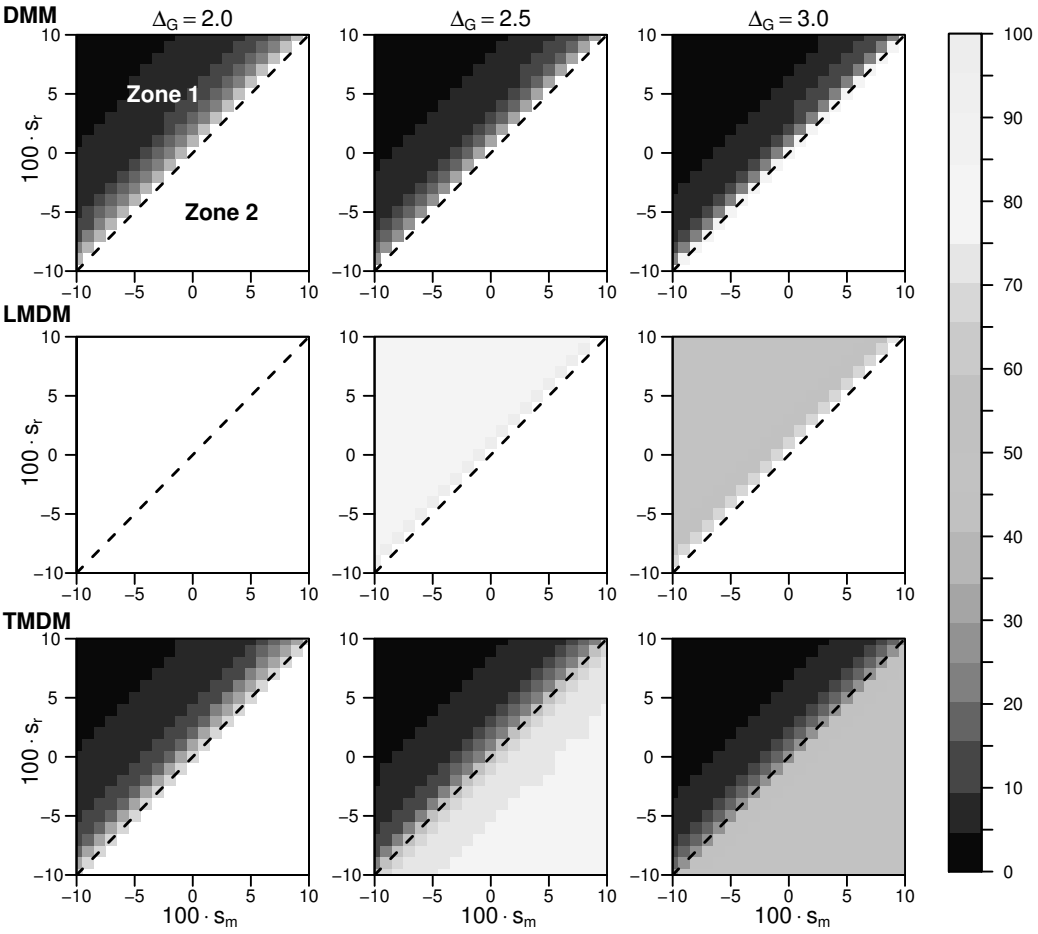

Figure 8. Sensitivity to selection parameters. Shaded maps indicate the age at which a superoxide concentration of $10^{-4}\,\mu$M is exceeded, given a model (rows), Δ_G (columns), and (s_m,s_r) coordinate point. Zone 1 defined by $s_r > s_m$, Zone 2 by $s_r < s_m$, with dashed line indicating Zone 1-Zone 2 barrier. Zone assignments are the same for all panels. Unshaded regions indicate a failure of superoxide concentrations to pass the threshold within the allotted 100-year period. For $\Delta_G \leqslant 2$ in the LMDM, the threshold is never reached. As Δ_G increases, the age to reach threshold decreases in all model formulations.

stress kinase c-Jun N-terminal kinase (JNK) in skeletal muscle cells [75]. JNK impairs insulin signaling by inhibiting insulin receptor substrate 1 (IRS-1) activity through serine phosphorylation [31, 32, 76]. This results in decreased tyrosine activity of IRS-1, which ultimately reduces insulin-mediated glucose uptake and hence insulin sensitivity. Thus, our models provide a foundation for modeling the contribution of superoxide production and mitochondrial defects in cellular IR.

The mitochondrial selection models (DMM, LMDM, and TMDM) reveal important characteristics of mitochondria that influence health and disease. The selection parameters, s_r and s_m, which respectively denote the relative difference in replication and turnover between mitochondrial classes, describe the interplay between the benefit and cost of the damaged state. Of the possible cases, damaged mitochondria are believed to be targeted for degradation more than their undamaged counterparts [24, 55, 77]. Under these circumstances, we restrict our discussion to the case in which $s_m > 0$. If $s_r < s_m$, persistence in the healthier Zone 2 is more likely, regardless of whether a replicative advantage or disadvantage exists. However, if internal mitochondrial dysfunction and population-level abnormalities are synergistic, as in the TMDM, sufficient levels of glucose intake can overpower any selective advantage of undamaged mitochondria within the average lifetime. Thus, the nature of the interaction between intrinsic and extrinsic mitochondrial characteristics can determine overall outcome.

The models can also mimic a variety of pathological states that exacerbate IR. Genetic predisposition can give rise to mitochondrial defects [78, 79]. Defective mitochondrial fusion induction has been detected in the severely insulin-resistant, early-onset type 2 diabetic population, wherein mitofusin 2 (Mfn2), an important protein in mitochondrial fusion, is repressed in skeletal muscle of type 2 diabetics [80]. Mfn2 deficiency has also been found to lead to mitochondrial dysfunction, oxidative stress and JNK activation in skeletal muscle [81]. PINK1 and Parkin regulate mitophagy of damaged mitochondria, and a recent report shows that Mfn2, possibly activated by PINK1, promotes mitophagy through Parkin binding in cardiac cells [77]. It is not yet established whether

this Mfn2 function applies to skeletal muscle mitochondria [82], but the implication would link reduced Mfn2 induction in insulin-resistant individuals and reduced sensitivity to mitophagic elimination of damaged organelles.

Within the framework of our models, genetic defects can be associated with a specific mode of interaction between intrinsic mitochondrial function and selection. More severe cases may result in synergy (TMDM), whereas less pathological cases may maintain class-specific dysfunction (LMDM). The relationship between the selection parameters are determined by the nature of the genetic defect. For example, Mfn2 deficiency may be represented by lower s_m values. Such a characterization can also give insight to the timing and severity of these processes. Thus, an individual with a defect in fusion activation in skeletal muscle may be more sensitive to changes in mitochondrial inefficiency, as in the TMDM, and may also have reduced autophagy of damaged mitochondria, resulting in decreased targeted turnover, a shift in the relationship between selection parameters, and increased dysfunction over time.

It has also been shown that while mitochondrial dysfunction can arise through ROS-mediated means in skeletal muscle, it is not necessarily the primary cause of IR in this tissue [83]. Our models are consistent with this idea, with increased glucose uptake resulting in the initiation of processes leading to increased ROS production and mitochondrial dysfunction. In this work, we use Δ_G as a surrogate for a high calorie diet and more generally, for the contribution of environmental factors to IR susceptibility. We eliminate systemic effects by assuming that with this elevated glucose input, uptake is increased accordingly. With this assumption, we modify the classical insulin sensitivity parameter s to achieve this goal, and remark that similar results may be obtained by a sufficient increase in basal insulin, maintained at a constant level (not shown). This latter circumstance would reflect preexisting hyperinsulinemic IR, serving as a sufficient condition for oxidative stress-mediated mitochondrial abnormalities. In this way, we examine the mechanisms in the current models as those which can maintain, but not necessarily initiate, skeletal muscle IR.

The nature of irreversible damage lies in a progression toward inevitable and

irreversible dysfunction. Clinically, the process can be sufficiently retarded to prevent disease onset within the course of a lifetime. This ability depends on the effectiveness of intervention strategies targeted toward individuals at high risk of developing type 2 diabetes or other metabolic diseases.

The open questions in IR pathogenesis require that we combine established and proposed physiological mechanisms of dysfunction in our models. Due to the complexity of the system, we make one particular set of assumptions about the feedback in the system, but recognize that other choices and quantitations of feedback are possible. Specifically, we use a linear function to define the impact of superoxide on the mitochondrial damage transition probability and include mitochondrial inefficiency as one of the state variables linking superoxide to its own production. Instead of the multiple mitochondrial damage classes with varying levels of dysfunction addressed by Kowald and Kirkwood [44], our model of mitochondrial damage includes just two mitochondrial classes. A more diverse mitochondrial landscape may alter the stationary distribution of mitochondrial classes, but we suspect that this complexity will not qualitatively alter our results.

The complex role of ATP in glucose metabolism and cellular respiration is also not captured in the present model. We include ATP only as a destination of electron transport activity, but it has cytosolic and mitochondrial effects that provide additional feedback to the intracellular system. An accumulation of cytosolic ATP indicates low energy use and can slow the rate of glycolysis, which in turn reduces the rate at which ATP can be produced in the mitochondrion [18]. This feedback allows the energy balance to be restored, while simultaneously limiting damage done by ROS. This protective mechanism would be maximally functional in cases of normal glucose intake. However, with increased glucose loads, glycolysis would occur more quickly and ATP-mediated inhibition would be reduced. Thus, with a combination of a sedentary lifestyle and nutrient overload, this mechanism may slow, but not stop, ROS production.

The intramitochondrial effects of lifestyle, diet, and ATP add an additional dimension to the problem. ATP is created from preexisting ADP in the mito-

chondrial matrix during cellular respiration. ATP must be transported to the cytosol for use by the cell, which occurs via a one-to-one exchange for ADP [18]. With minimal energy utilization, ATP accumulates, and ADP is depleted in the cytosol. With maximal glycolytic activity, the same occurs in the mitochondrial matrix. As a result, the potential energy generated by the proton gradient to power energy production is not released, which traps electrons in the ETC. These electrons are more likely to leak into the mitochondrial matrix and form superoxide. This imbalance is corrected only when enough protons have leaked across the inner membrane to decrease the electrochemical gradient, or when enough ATP has been used to allow ADP to be restored in the matrix [25]. ATP can therefore have both internal and population-level effects on mitochondria: Increased ATP production can retard electron transport in an individual organelle and can increase the cytosolic ATP that provides a global signal to all mitochondria.

IR in skeletal muscle is only one aspect of dysfunction in the pathway to diabetes. IR in other tissues, such as liver and adipose tissue, can induce additional dysfunction that may further hinder insulin signaling in muscle tissues, providing more complex mechanisms of feedback. Although we do not present an extended model of skeletal muscle IR here, we collectively use the current models to define a framework to answer how irreversible damage arising from environmental and genetic factors can slowly alter metabolic processes, on which molecular models further describing the progression of systemic IR and type 2 diabetes may be constructed.

5. Conclusions

A series of four models incorporating degrees of mitochondrial dysfunction predicts that mitochondrial heterogeneity and the persistence of abnormal function contributes to oxidative stress in skeletal muscle. Increased rate of glucose entry into cells can exacerbate stress by enhancing feedback between mitochondria and the superoxide they produce. The models predict that stress from

exogenous sources accelerates the progression toward dysfunction, without altering the trajectory. The models also provide a foundation on which insulin and stress signaling dynamics can be built, in order to address irreversible damage that includes plasma glucose and insulin dynamics, obesity-related dysfunction, β-cell failure, and long-term type 2 diabetes development.

Appendix A. Mitochondrial selection: Calculating the mean time to fixation

We classify the expected time to extinction of an undamaged mitochondrial population as the "time to total mitochondrial damage." We begin by reformulating the model of mitochondrial selection as a modified version of the classical gambler's ruin problem [84]. Let p_i and q_i denote the probabilities of net gain and loss of one undamaged mitochondrion, respectively. Then

$$\begin{aligned} p_i &= \frac{d_1(K-i)\cdot(1-\mu)b_0 i}{[d_0 i + d_1(K-i)][b_0 i + b_1(K-i)]} \\ q_i &= \frac{d_0 i\cdot[\mu b_0 i + b_1(K-i)]}{[d_0 i + d_1(K-i)][b_0 i + b_1(K-i)]}. \end{aligned} \tag{A.1}$$

Let W_i be the probability that, beginning with $M_0 = i$, M_0 will equal K before it reaches zero. Necessarily, this means $W_K = \mu W_{K-1}$. In general,

$$W_i = p_i W_{i+1} + q_i W_{i-1}. \tag{A.2}$$

Let L_i be the probability that all undamaged mitochondria will be lost before reaching a size of K from $M_0 = i$. Using Eq. (A.2), we obtain

$$L_i = (1 - p_i - q_i) + p_i L_{i+1} + q_i L_{i-1}. \tag{A.3}$$

Now, let T_i be the expected time until the undamaged population meets its ruin from a population of i mitochondria, and let E_i be the average duration of time between events. Because turnover events dictate the net changes in the

UU IR Author Manuscript

mitochondrial population,

$$E_i = [d_0 i + d_1(K - i)]^{-1}. \tag{A.4}$$

If M_0 remains unchanged, the new time to ruin is $T_i + E_i$. Similarly, the corresponding times for a gain or loss of healthy mitochondria are $T_{i+1} + E_i$ and $T_{i-1} + E_i$, respectively. These lead to the second-order difference equation

$$q_i T_{i-1} - (p_i + q_i)T_i + p_i T_{i+1} = -E_i, \tag{A.5}$$

with $T_0 = 0$. Eq. (A.5) can be solved explicitly to give

$$\begin{cases} T_i = T_0 + \displaystyle\sum_{j=0}^{i-1} \left[\eta_{j+1} + \sum_{m=0}^{K-j-2} \prod_{n=m+1}^{K-j-1} \eta_{K-m}\, \rho_{K-n} \right], \\ \qquad i = 1, \ldots, K-1, \\ T_K = \eta_K + T_{K-1}, \end{cases} \tag{A.6}$$

where $\eta_i = E_i/q_i$, and $\rho_i = p_i/q_i$. Using the parameters in Table 2, about 400 years would pass before total damage occurs in a population with K initially undamaged mitochondria under null selection.

Acknowledgements

Special thanks to James F. Selgrade for the helpful comments. EJG was supported by NSF grants DMS-0354259 at the University of Utah and DMS-0946431 at North Carolina State University.

References

[1] International Diabetes Federation, IDF Diabetes Atlas, International Diabetes Federation, fifth edition, 2011.

[2] D. Whiting, L. Guariguata, C. Weil, J. Shaw, IDF diabetes atlas: global

UU IR Author Manuscript

estimates of the prevalence of diabetes for 2011 and 2030, Diabetes research and clinical practice (2011).

[3] G. C. Weir, S. Bonner-Weir, Five stages of evolving β-cell dysfunction during progression to diabetes, Diabetes 53 (2004) S16–S21.

[4] T. Kadowaki, Insights into insulin resistance and type 2 diabetes from knockout mouse models, J. Clin. Invest. 106 (2000) 459–465.

[5] S. H. Back, R. J. Kaufman, Endoplasmic reticulum stress and type 2 diabetes, Annu. Rev. Biochem. 81 (2012) 16.1–16.27.

[6] D. M. Muoio, C. B. Newgard, Molecular and metabolic mechanisms of insulin resistance and β-cell failure in type 2 diabetes, Nat. Rev. Mol. Cell Biol. 9 (2008) 193–205.

[7] C. J. Rhodes, Type 2 diabetes—a matter of β-cell life and death?, Science 307 (2005) 380–384.

[8] J. L. Leahy, Pathogenesis of type 2 diabetes mellitus, Arch. Med. Res. 36 (2005) 197–209.

[9] C. J. Nolan, P. Damm, M. Prentki, Type 2 diabetes across generations: from pathophysiology to prevention and management, Lancet 378 (2011) 169–181.

[10] K. L. Hoehn, A. B. Salmon, C. Hohnen-Behrens, N. Turner, A. J. Hoy, G. J. Maghzal, R. Stocker, H. Van Remmen, E. W. Kraegen, G. J. Cooney, A. R. Richardson, D. E. James, Insulin resistance is a cellular antioxidant defense mechanism, Proc. Natl. Acad. Sci. 106 (2009) 17787–17792.

[11] M. A. Abdul-Ghani, R. A. DeFronzo, Pathogenesis of insulin resistance in skeletal muscle, J. Biomed. Biotechnol. 2010 (2010) 1–19.

[12] R. A. DeFronzo, Pathogenesis of type 2 diabetes mellitus, Med. Clin. N. Am. 88 (2004) 787–835.

[13] I. Fridovich, Superoxide radical and superoxide dismutases, Annu. Rev. Biochem. 64 (1995) 97–112.

[14] T. Tiganis, Reactive oxygen species and insulin resistance: the good, the bad and the ugly, Trends Pharmacol. Sci. 32 (2011) 82–89.

[15] A. J. Kowaltowski, A. E. Vercesi, Mitochondrial damage induced by conditions of oxidative stress, Free Radic. Biol. Med. 26 (1999) 463–471.

[16] A. Berdichevsky, L. Guarente, A. Bose, Acute oxidative stress can reverse insulin resistance by inactivation of cytoplasmic JNK, J. Biol. Chem. 285 (2010) 21581–21589.

[17] J. A. M. Smeitink, R. C. A. Sengers, J. M. F. Trijbels (Eds.), Oxidative phosphorylation in health and disease, Landes Bioscience/Eureka.com; Kluwer Academic/Plenum Publishers, 2004.

[18] H. Lodish, A. Berk, P. Matsudaira, C. A. Kaiser, M. Krieger, M. P. Scott, S. L. Zipursky, J. Darnell, Molecular Cell Biology, W.H. Freeman and Company, 2004.

[19] M. P. Murphy, How mitochondria produce reactive oxygen species, Biochem. J. 417 (2009) 1–13.

[20] N. M. Druzhyna, G. L. Wilson, S. P. LeDoux, Human mitochondrial mutations and repair, in: Plant Mitochondria, Springer Science + Business Media, 2011, pp. 493–521.

[21] S. Marchi, C. Giorgi, J. M. Suski, C. Agnoletto, A. Bononi, M. Bonora, E. De Marchi, S. Missiroli, S. Patergnani, F. Poletti, A. Rimessi, J. Duszynski, M. R. Wieckowski, P. Pinton, Mitochondria-Ros crosstalk in the control of cell death and aging, J. Sig. Transduc. 2012 (2012) 1–17.

[22] Z. Cao, J. Wanagat, S. H. McKiernan, J. M. Aiken, Mitochondrial DNA deletion mutations are concomitant with ragged red regions of individual,

aged muscle fibers: analysis by laser-capture microdissection, Nucleic acids research 29 (2001) 4502–4508.

[23] G. Fayet, M. Jansson, D. Sternberg, A.-R. Moslemi, P. Blondy, A. Lombès, M. Fardeau, A. Oldfors, Ageing muscle: clonal expansions of mitochondrial DNA point mutations and deletions cause focal impairment of mitochondrial function, Neuromuscular Disorders 12 (2002) 484–493.

[24] I. Kim, S. Rodriguez-Enriquez, J. J. Lemasters, Selective degradation of mitochondria by mitophagy, Arch. Biochem. Biophys. 462 (2007) 245–253.

[25] D. C. Wallace, A mitochondrial paradigm of metabolic degenerative diseases, aging, and cancer: a dawn for evolutionary medicine, Annu. Rev. Genet. 39 (2005) 359–407.

[26] A. K. Holley, V. Bakthavatchalu, J. M. Velez-Roman, D. K. St. Clair, Manganese superoxide dismutase: guardian of the powerhouse, Int. J. Mol. Sci. 12 (2011) 7114–7162.

[27] J. J. Lemasters, Selective mitochondrial autophagy, or mitophagy, as a targeted defense against oxidative stress, mitochondrial dysfunction, and aging, Rejuvenation Res. 8 (2005) 3–5.

[28] R. J. Youle, A. M. van der Bliek, Mitochondrial fission, fusion, and stress, Science 337 (2012) 1062–1065.

[29] A. D. De Grey, A proposed refinement of the mitochondrial free radical theory of aging, Bioessays 19 (1997) 161–166.

[30] A. Terman, U. T. Brunk, Myocyte aging and mitochondrial turnover, Exp. Gerontol. 39 (2004) 701–705.

[31] V. Aguirre, T. Uchida, L. Yenush, R. Davis, M. F. White, The c-Jun N-terminal kinase promotes insulin resistance during association with insulin receptor substrate-1 and phosphorylation of Ser^{307}, J. Biol. Chem. 275 (2000) 9047–9054.

[32] J. Hirosumi, G. Tuncman, L. Chang, C. Z. Görgun, K. T. Uysal, K. Maeda, M. Karin, G. S. Hotamisligil, A central role for JNK in obesity and insulin resistance, Nature 420 (2002) 333–336.

[33] B. Topp, K. Promislow, G. deVries, R. M. Miura, D. T. Finegood, A model of β-cell mass, insulin, and glucose kinetics: pathways to diabetes, J. Theor. Biol. 206 (2000) 605–619.

[34] A. De Gaetano, T. Hardy, B. Beck, E. Abu-Raddad, P. Palumbo, J. Bue-Valleskey, N. Pørksen, Mathematical models of diabetes progression, Am. J. Physiol. Endocrinol. Metab. 295 (2008) E1462–E1479.

[35] R. N. Bergman, Minimal model: Perspective from 2005, Horm. Res. 64 (2005) 8–15.

[36] J. Henquin, Triggering and amplifying pathways of regulation of insulin secretion by glucose., Diabetes 49 (2000) 1751–1760.

[37] W. Malaisse, J. Hutton, S. Kawazu, A. Herchuelz, I. Valverde, A. Sener, The stimulus-secretion coupling of glucose-induced insulin release, Diabetologia 16 (1979) 331–341.

[38] M. Brissova, M. Shiota, W. Nicholson, M. Gannon, S. Knobel, D. Piston, C. Wright, A. Powers, Reduction in pancreatic transcription factor PDX-1 impairs glucose-stimulated insulin secretion, J. Biol. Chem. 277 (2002) 11225–11232.

[39] P. Maechler, C. Wollheim, Mitochondrial glutamate acts as a messenger in glucose-induced insulin exocytosis, Nature 402 (1999) 685–689.

[40] J. G. Scandalios, Oxidative stress and the molecular biology of antioxidant defenses, Cold Spring Harbor Laboratory, 1997.

[41] B. Warner, L. Stuart, S. Gebb, J. Wispe, Redox regulation of manganese superoxide dismutase, Am. J. Physiol. Lung Cell. Mol. Physiol. 271 (1996) L150–L158.

[42] L. Miao, D. K. S. Clair, Regulation of superoxide dismutase genes: implications in disease, Free Radic. Biol. Med. 47 (2009) 344–356.

[43] G. Pani, O. R. Koch, T. Galeotti, The p53-p66shc-Manganese superoxide dismutase (MnSOD) network: A mitochondrial intrigue to generate reactive oxygen species, Int. J. Biochem. Cell Biol. 41 (2009) 1002–1005.

[44] A. Kowald, T. B. L. Kirkwood, A network theory of ageing: the interactions of defective mitochondria, aberrant proteins, free radicals and scavengers in the ageing process, Mutat. Res. 316 (1996) 209–236.

[45] A. E. Brynes, J. Adamson, A. Dornhorst, G. S. Frost, The beneficial effect of a diet with low glycaemic index on 24 h glucose profiles in healthy young people as assessed by continuous glucose monitoring, Brit. J. Nutr. 93 (2005) 179–182.

[46] A. E. Brynes, J. L. Lee, R. E. Brighton, A. R. Leeds, A. Dornhorst, G. S. Frost, A low glycemic diet significantly improves the 24-h blood glucose profile in people with type 2 diabetes, as assessed using the continuous glucose MiniMed monitor, Diabetes Care 26 (2003) 548–549.

[47] G. Freckmann, S. Hagenlocher, A. Baumstark, N. Jendrike, R. C. Gillen, K. Rössner, C. Haug, Continuous glucose profiles in healthy subjects under everyday life conditions and after different meals, J. Diabetes Sci. Technol. 1 (2007) 695.

[48] P. Mecocci, G. Fano, S. Fulle, U. MacGarvey, L. Shinobu, M. C. Polidori, A. Cherubini, J. Vecchiet, U. Senin, M. F. Beal, Age-dependent increases in oxidative damage to DNA, lipids, and proteins in human skeletal muscle, Free Radic. Biol. Med. 26 (1999) 303–308.

[49] R. J. Youle, D. P. Narendra, Mechanisms of mitophagy, Nat. Rev. Mol. Cell Biol. 12 (2011) 9–14.

[50] K. Khrapko, J. Vijg, Mitochondrial DNA mutations and aging: devils in the details?, Trends Genet. 25 (2009) 91–98.

[51] N.-G. Larsson, Somatic mitochondrial DNA mutations in mammalian aging, Annu. Rev. Biochem. 79 (2010) 683–706.

[52] M. Zoratti, I. Szabó, The mitochondrial permeability transition, Biochim. Biophys. Acta 1241 (1995) 139–176.

[53] R. Scherz-Shouval, Z. Elazar, ROS, mitochondria and the regulation of autophagy, Trends Cell Biol. 17 (2007) 422–427.

[54] E. Renshaw, Stochastic population processes: analysis, approximations, simulations, Oxford University Press, 2011.

[55] J. Lee, G. Samantha, J. Zhang, Autophagy, mitochondria and oxidative stress: cross-talk and redox signalling, Biochem. J. 441 (2012) 523–540.

[56] C. Gardiner, Stochastic methods: a handbook for the natural and social sciences, volume 4, Springer, 2009.

[57] M. Z. Shrayyef, J. E. Gerich, Normal glucose homeostasis, in: Principles of Diabetes Mellitus, Springer, 2010, pp. 19–35.

[58] K. Zierler, Whole body glucose metabolism, Am. J. Phys. Endocrinol. Metab. 276 (1999) E409–E426.

[59] G. Buettner, C. Ng, M. Wang, V. Rodgers, F. Schafer, A new paradigm: Manganese superoxide dismutase influences the production of H_2O_2 in cells and thereby their biological state, Free Radic. Biol. Med. 41 (2006) 1338–1350.

[60] J. F. Turrens, Mitochondrial formation of reactive oxygen species, J. Physiol. 552 (2003) 335–344.

[61] M. Byrne, J. Sturis, K. Polonsky, Insulin secretion and clearance during low-dose graded glucose infusion, Am. J. Physiol. Endocrinol. Metab. 268 (1995) E21–E27.

[62] S. K. Poovathingal, J. Gruber, B. Halliwell, R. Gunawan, Stochastic drift in mitochondrial DNA point mutations: a novel perspective *ex silico*, PLoS Comp. Bio. 5 (2009) e10000572.

[63] W. Duckworth, R. Bennett, F. Hamel, Insulin degradation: progress and potential, Endocr. Rev. 19 (1998) 608.

[64] R. L. Lieber, Skeletal muscle structure, function, and plasticity: the physiological basis of rehabilitation, Lippincott Williams & Wilkins, third edition, 2010.

[65] P. Schantz, E. Randall-Fox, W. Hutchison, A. Tydén, P. Åstrand, Muscle fibre type distribution, muscle cross-sectional area and maximal voluntary strength in humans, Acta Physiol. Scand. 117 (1983) 219–226.

[66] A. Kaasik, D. Safiulina, A. Zharkovsky, V. Veksler, Regulation of mitochondrial matrix volume, Am. J. Physiol. Cell Physiol. 292 (2007) C157–C163.

[67] F. Åberg, E.-L. Appelkvist, G. Dallner, L. Ernster, Distribution and redox state of ubiquinones in rat and human tissues, Arch. Biochem. Biophys. 295 (1992) 230–234.

[68] R. A. Menzies, P. H. Gold, The turnover of mitochondria in a variety of tissues of young adult and aged rats, J. Biol. Chem. 246 (1971) 2425–2429.

[69] J. L. Evans, I. D. Goldfine, B. A. Maddux, G. M. Grodsky, Oxidative stress and stress-activated signaling pathways: a unifying hypothesis of type 2 diabetes, Endocr. Rev. 23 (2002) 599–622.

[70] J. Kim, Y. Wei, J. R. Sowers, Role of mitochondrial dysfunction in insulin resistance, Circ. Res. 102 (2008) 401–414.

[71] M. Valko, D. Leibfritz, J. Moncol, M. T. D. Cronin, M. Mazur, J. Telser, Free radicals and antioxidants in normal physiological functions and human disease, Int. J. Biochem. Cell. Biol. 39 (2007) 44–84.

[72] T. Finkel, Signal transduction by reactive oxygen species, J. Cell Biol. 194 (2011) 7–15.

[73] Y. C. Jang, H. Van Remmen, The mitochondrial theory of aging: insight from transgenic and knockout mouse models, Exp. Gerontol. 44 (2009) 256–260.

[74] A. Y. Seo, A. Joseph, D. Dutta, J. C. Y. Hwang, J. P. Aris, C. Leeuwenburgh, New insights into the role of mitochondria in aging: mitochondrial dynamics and more, J. Cell Sci. 123 (2010) 2533–2542.

[75] M. Yoshizumi, J. Abe, J. Haendeler, Q. Huang, B. C. Berk, Src and Cas mediate JNK activation but not ERK1/2 and p38 kinases by reactive oxygen species, J. Biol. Chem. 275 (2000) 11706–11712.

[76] K. Hiratani, T. Haruta, A. Tani, J. Kawahara, I. Usio, M. Kobayashi, Roles of mTOR and JNK in serine phosphorylation, translocation, and degradation of IRS-1, Biochem. Biophys. Res. Commun. 335 (2005) 836–842.

[77] Y. Chen, G. W. Dorn, PINK1-phosphorylated mitofusin 2 is a Parkin receptor for culling damaged mitochondria, Science 340 (2013) 471–475.

[78] M. E. Patti, A. J. Butte, S. Crunkhorn, K. Cusi, R. Berria, S. Kashyap, Y. Miyazaki, I. Kohane, M. Costello, R. Saccone, E. J. Landaker, A. B. Goldfine, E. Mun, R. DeFronzo, J. Finlayson, C. R. Kahn, L. J. Mandarino, Coordinated reduction of genes of oxidative metabolism in humans with insulin resistance and diabetes: potential role of PGC1 and NRF1, Proc. Nat. Acad. Sci. 100 (2003) 8466–8471.

[79] K. F. Petersen, S. Dufour, D. Befroy, R. Garcia, G. I. Shulman, Impaired mitochondrial activity in the insulin-resistant offspring of patients with type 2 diabetes, New Engl. J. Med. 350 (2004) 664–671.

[80] M. I. Hernández-Alvarez, H. Thabit, N. Burns, S. Shah, I. Brema, M. Hatunic, F. Finucane, M. Liesa, C. Chiellini, D. Naon, A. Zorzano, J. J. Nolan,

Subjects with early-onset type 2 diabetes show defective activation of the skeletal muscle PGC-1α/mitofusin-2 regulatory pathway in response to physical activity, Diabetes Care 33 (2010) 645–651.

[81] D. Sebastián, M. I. Hernández-Alvarez, J. Segalés, E. Sorianello, J. P. Muñoz, D. Sala, A. Waget, M. Liesa, J. C. Paz, P. Gopalacharyulu, M. Orečič, S. Pich, R. Burcelin, M. Palacín, A. Zorzano, Mitofusin 2 (Mfn2) links mitochondrial and endoplasmic reticulum function with insulin signaling and is essential for normal glucose homeostasis, Proc. Nat. Acad. Sci. 109 (2012) 5523–5528.

[82] L. Pallanck, Mitophagy: Mitofusin recruits a mitochondrial killer, Curr. Biol. 23 (2013) R570–R572.

[83] C. Bonnard, A. Durand, S. Peyrol, E. Chanseaume, M. Chauvin, B. Morio, H. Vidal, J. Rieusset, Mitochondrial dysfunction results from oxidative stress in the skeletal muscle of diet-induced insulin-resistant mice, J. Clin. Invest. 118 (2008) 789–800.

[84] A. Munford, S. Lewis, A note on gambler's ruin against an infinitely rich adversary, Internat. J. Math. Ed. Sci. Tech. 12 (1981) 165–168.